Amine-Modified Graphene: Thrombo-Protective Safer Alternative to Graphene Oxide for Biomedical Applications

Sunil K. Singh,[†] Manoj K. Singh,[‡] Paresh P. Kulkarni,[†] Vijay K. Sonkar,[†] José J. A. Grácio,[‡] and Debabrata Dash[†,*]

[†]Department of Biochemistry, Institute of Medical Sciences, Banaras Hindu University, Varanasi 221005, India, and [‡]Center for Mechanical Technology & Automation, University of Aveiro, Aveiro-3810-193, Portugal

ABSTRACT Graphene and its derivatives have attracted significant research interest based on their application potential in different fields including biomedicine. However, recent reports from our laboratory and elsewhere have pointed to serious toxic effects of this nanomaterial on cells and organisms. Graphene oxide (GO) was found to be highly thrombogenic in mouse and evoked strong aggregatory response in human platelets. As platelets play a central role in hemostasis and thrombus formation, thrombotoxicity of GO potentially limits its biomedical applications. Surface chemistry of nanomaterials is a critical determinant of biocompatibility, and thus differentially functionalized nanomaterials exhibit varied cellular toxicity. Amine-modified carbon nanotubes have recently been shown to possess cytoprotective action, which was not exhibited by their relatively toxic carboxylated counterparts. We, therefore, evaluated the effect of amine modification of graphene on platelet reactivity. Remarkably, our results revealed for the first time that amine-modified graphene (G-NH_2) had absolutely no stimulatory effect on human platelets nor did it induce pulmonary thromboembolism in mice following intravenous administration. Further, it did not evoke lysis of erythrocytes, another major cellular component in blood. These findings contrasted strikingly the observations with GO and reduced GO (RGO). We conclude that G-NH_2 is not endowed with thrombotoxic property unlike other commonly investigated graphene derivatives and is thus potentially safe for *in vivo* biomedical applications.

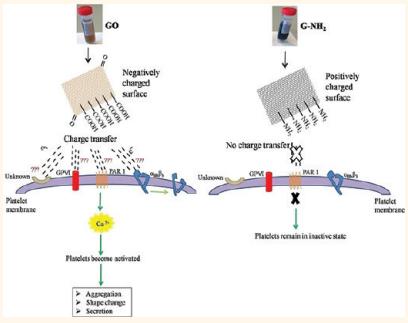

KEYWORDS: amine-modified graphene · graphene oxide · thrombus · surface charge distribution · hemolysis · thromboembolism

Among various nanomaterials, graphene, a novel carbon-based nanomaterial, has attracted a great deal of attention due to its remarkable physical, chemical, and biological characteristics. The distinct structural properties of graphene, in particular, its high aspect ratio, propensity for functional modification, unique electronic and optical properties, as well as potential biocompatibility, render it an attractive candidate for biomedical applications such as biosensor development, imaging, drug delivery, bacterial inhibition, and photothermal therapy.[1−9]

For biomedical and pharmaceutical applications, it is extremely important that graphene preparation should be biocompatible, water-dispersible, and nontoxic. These attributes are achievable by appropriate chemical functionalization of graphene, which enables graphene sheets to be well-dispersed in a range of polar solvents and particularly well in water.[3,5,10,11] In recent years, graphene oxide (GO), a heavily oxygenated graphene derivative having high stability in aqueous dispersion, has been profoundly explored for biomedical applications such as *in vitro* drug delivery[4,5] and cellular imaging.[3,4] GO has also been employed as a drug carrier for controlled loading and release of antitumor agents.[12,13] Further, GO has been projected as a novel biosensing platform for detection of various biomolecules.[14−17] Beyond that, due to strong optical absorption in the near-infrared range, GO can lead to photothermal ablation of tumors following intravenous administration in animals.[8,9] Unlike other carbon-based nanomaterials, biomedical applications of graphene have grown at a rapid pace and exhibit immense potential for the future.

Platelets are central players in the maintenance of hemostasis and blood clotting. Platelets remain "hyperactive" in thrombotic disorders like coronary artery diseases, stroke, and diabetes mellitus and play a critical role in their pathogenesis.[18−21] We have recently shown that GO can evoke

* Address correspondence to ddass@satyam.net.in.

Received for review January 13, 2012 and accepted February 29, 2012.

Published online February 29, 2012
10.1021/nn300172t

strong aggregatory response in human platelets in a scale comparable to that elicited by thrombin, one of the most potent physiological agonists of platelets.[22] Further, when administered intravenously into mouse, GO triggered extensive pulmonary thromboembolism consistent with pro-thrombotic nature of this nanomaterial, while considerably less negatively charged reduced GO (RGO) elicited only minor aggregatory response. There have been reports from other laboratories, too, underscoring cytotoxicity of GO.[6,7,23−28] So, these findings raise an alarm on putative biomedical applications of GO and RGO in the form of drug delivery, cellular imaging, cancer photothermal therapy, and diagnostic tools.

This encouraged us to search for alternative chemical derivatives of graphene with similar physical attributes, which are well-dispersed in a range of solvents and have minimal or low thrombogenic potential. To date, amine-functionalized graphene (G-NH_2) has not been studied for biomedical applications, while amine-modified single-walled carbon nanotubes were recently shown to be cytoprotective toward neuronal cells.[29,30] Here we report for the first time that positively charged G-NH_2 is more biocompatible than GO. Contrasting the earlier observations with GO and RGO, G-NH_2 neither demonstrates stimulatory action toward platelets nor induces pulmonary thromoembolism in mice. Further, G-NH_2 was also found to be more hemocompatible as compared to GO which induced significant hemolysis. Thus, G-NH_2 can be a far safer alternative to the oxygenated derivative of graphene, with potential biomedical applications in areas such as imaging, drug delivery, as well as photothermal therapy.

RESULTS AND DISCUSSION

Characterization of G-NH_2. G-NH_2 was derived from GO sheets by replacing carboxyl groups with amine as detailed in the Methods section. Following amine functionalization, an aqueous solution of graphene turned darker as compared to GO (Figure 1a, lower panel). FTIR spectrum of G-NH_2 exhibited the characteristic peak at 1573 cm^{-1} corresponding to N−H in-plane (Figure 1c). Further broadening of peak in the range of 950−1250 cm^{-1} that corresponds to the C−N bond stretching was also observed (Figure 1c).[31,32] Besides, the peak at ∼1735 cm^{-1} attributable to C═O stretch of the carboxylic (COOH) group was absent in the FTIR spectrum of G-NH_2 (Figure 1b,c).

High-resolution transmission electron microscopy (HR-TEM) studies were performed to examine crystallinity and quality of as-synthesized G-NH_2 sheets. For this, samples were prepared by dipping carbon-coated copper grids into the G-NH_2 suspension and allowing them to dry. Figure 2b represents a bright-field TEM image of the G-NH_2 sheet attached to a copper grid. The suspended graphene−amine membrane consisted of single- or few-layer sheets with average dimension of 2 μm. The HR-TEM image of this suspended sheet (within the red region in Figure 2b) is presented in Figure 2c. The inset in Figure 2c represents the fast Fourier transform (FFT) of the red region, which supports the crystalline nature of few-layer graphene sheets. Figure 2d reveals the FFT image of Figure 2c after filtering in the frequency domain to remove unwanted noise for clarity. From the above observations, we conclude that structural morphology and crystalline nature of graphene sheets remained unchanged during transformation of COOH groups into amine species.

Raman spectroscopy is a widely used characterization tool to evaluate the nature of disorder and defects on carbon-based nanomaterials. Raman spectra of GO and G-NH_2 exhibited prominent graphite peaks, also known as "G band", at 1580 cm^{-1} (Supporting Information Figure S1). Emergence of defects on graphene sheets upon functionalization was evident from the prominent D band at 1350 cm^{-1} and broadening of D and G peaks. The intensity ratio of D/G peaks became larger, which further indicates increased disorder in graphene lattice. However, we found equivalent defects on GO and G-NH_2, as reflected from similar D band intensities and D/G ratio. Recent reports by other investigators have also demonstrated nearly equal crystallite size and similar defect characteristics of GO and G-NH_2.[33]

We also carried out zeta-potential measurements to evaluate the surface charge on graphene sheets (Supporting Information Figure S2). The results showed that GO sheets were highly negatively charged in the pH range between 3.5 and 9, which could be attributed to the presence of −COOH groups on the surface of these materials. On the other hand, G-NH_2 exhibited characteristics in support of positive charge in the pH regime below ∼10. We observed amphoteric characteristics under a higher pH environment, which could be due to the residual carboxylic acid groups as discussed elsewhere.[34] RGO nanosheets exhibited zeta-potential values near zero for the same pH range, which was consistent with reduction in oxygen functionality on the surface. Optical properties of graphene derivatives were further characterized by UV−vis−NIR spectroscopy (Supporting Information Figure S3). The main absorbance peak attributable to $\pi-\pi^*$ transitions of C═C in as-synthesized GO occurred at around ∼230 nm, which was red-shifted to ∼260 nm in RGO, suggestive of revival of electronic conjugation within graphene sheets upon reduction of GO. A shoulder around 320 nm in both as-synthesized GO as well as RGO may be attributable to $n-\pi^*$ transitions of C═O. In the case of G-NH_2, we observed consistently higher absorbance in the entire visible and NIR regions

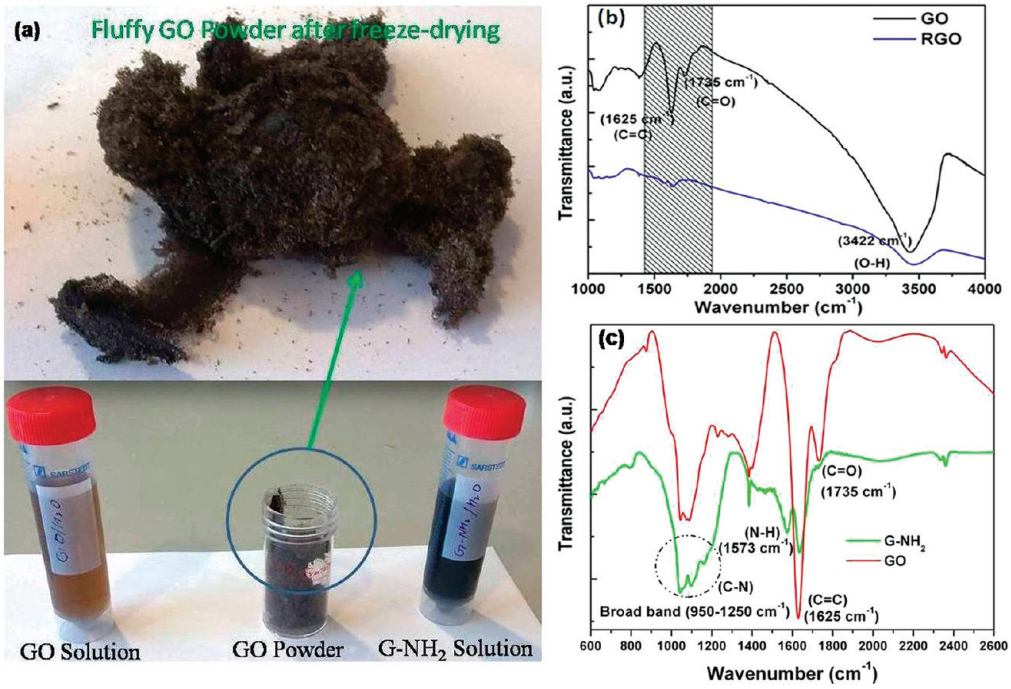

Figure 1. Characterization of G-NH_2. (a) Upper panel, GO powder obtained after freeze-drying. Lower panel, aqueous solutions of purified GO and G-NH_2. (b,c) FTIR spectra of GO, RGO, and G-NH_2 as indicated.

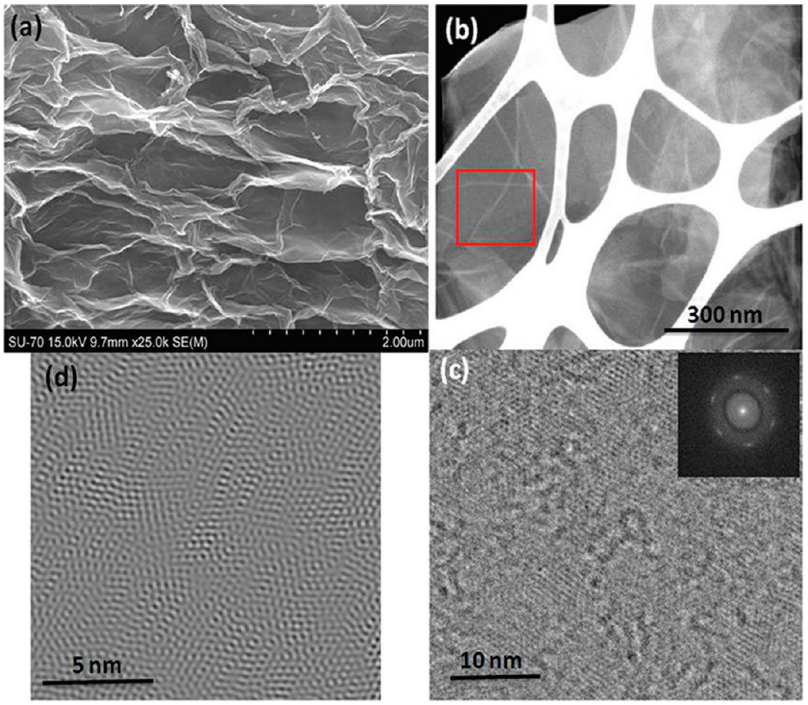

Figure 2. Electron microscopic characterization of G-NH_2. (a) SEM image of aqueous solution of purified GO. (b) Bright-field TEM image of suspended G-NH_2 sheet on carbon-coated copper grid. (c) HR-TEM image of the suspended graphene–amine sheet (in the red bounded region in panel b). An FFT (inset of panel c) was performed in the red bounded region of panel b, exhibiting perfect crystallinity of the GO sheet. (d) Reconstructed image of panel c by filtering in the frequency domain to remove unwanted noise for more clarification.

compared to other derivatives of graphene under this study.

For flow cytometric analysis, forward (FSC) and side (SSC) scatter parameters of GO, G-NH_2, and RGO were acquired in the dot as well as contour plot acquisition quadrants (Supporting Information Figure S4). Sheath fluid was mobilized to determine the background noise. By adjusting FSC and SSC detector voltages to

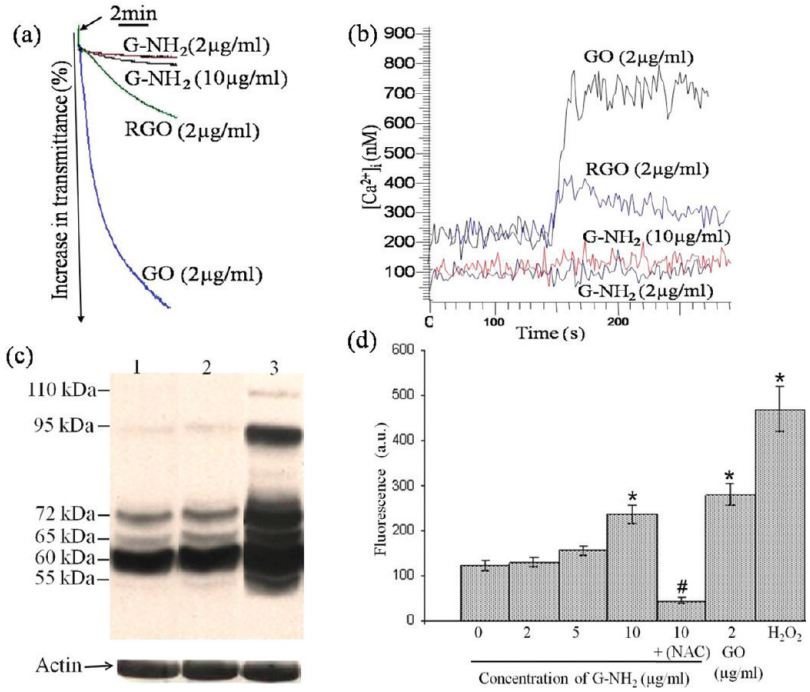

Figure 3. Differential effects of GO, RGO and G-NH_2 on human platelets. (a) Platelet aggregation induced by GO, RGO, and G-NH_2 at indicated concentrations. (b) Intracellular calcium flux in Fura-2-loaded platelets treated with graphene derivatives in the presence of extracellular calcium (1 mM). (c) Effect of graphene derivatives on platelet tyrosine phosphoproteome. Lane 1, resting platelets; lane 2, G-NH_2 (10 μg/mL)-treated platelets; and lane 3, GO (2 μg/mL)-treated stirred (aggregated) platelets. (d) ROS generation in H_2DCF-loaded platelets treated with different concentrations of G-NH_2, GO, H_2O_2 (10 μM), NAC (1 μM), or vehicle, as indicated. Results are representative of five independent experiments (mean $\pm$ SD) (*p < 0.05 as compared with control group, #p < 0.05 as compared with 10 μM G-NH_2).

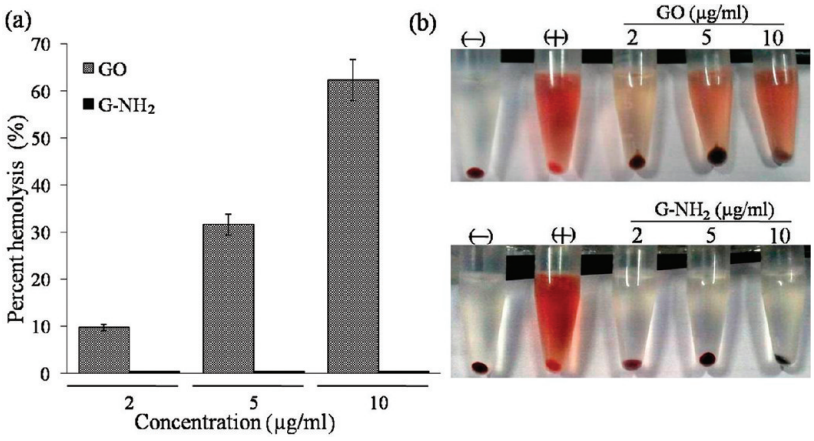

Figure 4. Effect of G-NH_2 on erythrocyte membrane integrity. (a) Percent hemolysis of RBCs incubated with different concentrations (2, 5, and 10 μg/mL) of G-NH_2 or GO as indicated. Data represent mean $\pm$ SD from three independent experiments. (b) RBC suspensions were exposed to varying concentrations (2, 5, and 10 μg/mL) of G-NH_2 or GO for 3 h followed by centrifugation. Red color of supernatant indicates hemolysis; (+) and (−) symbols represent positive (RBCs suspended in deionized water) and negative (RBCs suspended in phosphate buffered saline (PBS) controls, respectively.

E00 and 350 V, respectively, the majority of GO, RGO, and G-NH_2 populations was found to be confined in the upper quadrants (Supporting Information Figure S4) reasonably well distanced from background noise. Identical gating was imposed on differentially functionalized graphene populations. The innermost contours (representing more than 80% population in each graphene species) were found to be located in upper left quadrants (Supporting Information Figure S4d−f), consistent with identical size distribution of different graphene derivatives irrespective of the nature of surface functionalization.

GO sheets are known to be endowed with intrinsic fluorescence detectable on the FL3 channel (excited with 488 nm laser, while emission measured with 670 nm long pass filter) of the flow cytometer.[22,35]

Next, we investigated the effect of amine modification on fluorescence properties of graphene. In sharp contrast to the observations made with GO, the amine derivative of graphene was nonfluorescent in the FL3 region (Supporting Information Figure S5a). RGO also had negligible fluorescence similar to G-NH_2. To further validate flow cytometry-based observations, we evaluated the fluorescence property of graphene derivatives by fluorescence spectroscopy. Fluorescence emission spectra of GO displayed a characteristic peak at 575 nm when excited at 400 nm,[35,36] while G-NH_2 and RGO exhibited no detectable fluorescence (Supporting Information Figure S5b). We conclude that GO is the only fluorescent species among different graphene derivatives.

Effect of G-NH_2 on Platelet Functions. We have recently demonstrated that GO can potentially induce integrin-mediated platelet aggregation under both *in vitro* and *in vivo* situations in a scale comparable to that elicited by thrombin, one of the most potent physiological agonists of platelets.[22] In keeping with this observation, addition of GO (2 μg/mL) to a suspension of freshly isolated human platelets ($0.5-0.8 \times 10^9$ cells/mL) triggered a strong wave of cell aggregation (amplitude $90 \pm 5\%$) (Figure 3a). However, at identical concentration, aggregation elicited by RGO dropped to $15 \pm 2\%$ (Figure 3a). Strikingly, 2 μg/mL of G-NH_2 failed to induce platelet aggregation, while at 5 times higher concentration (10 μg/mL), it could evoke only a minor wave of transmittance (amplitude $8 \pm 0.5\%$) (Figure 3a), consistent with a determining role of graphene surface functionalization/charge distribution in platelet stimulation.

In order to understand molecular underpinnings of the above observations, we explored the effect of G-NH_2 on platelet intracellular Ca^{2+}, $[Ca^{2+}]_i$, reactive oxygen species (ROS), and state of platelet tyrosine phosphoproteome, which are critical determinants of intracellular signaling impacting platelet functions. GO-induced platelet activation had been attributed to release of intracellular free calcium from the cytosolic stores.[22] In line with this, GO (2 μg/mL) evoked an initial rise in $[Ca^{2+}]_i$ by more than 4-fold the resting value followed by plateau, while RGO (2 μg/mL) induced nearly 2-fold rise in intracellular calcium (Figure 3b). However and quite strikingly, G-NH_2 (2 and 10 μg/mL) had absolutely no effect on intracellular calcium flux (Figure 3b).

GO-induced platelet reactivity is associated with phosphorylation of multiple cytosolic proteins on tyrosine residues.[22] In order to examine the effect of G-NH_2, we studied the profile of tyrosine phosphorylated proteins in platelets exposed to different graphene derivatives. As expected, GO evoked a strong wave of tyrosine phosphorylation on multiple proteins (Figure 3c, lane 3). G-NH_2 (10 μg/mL), on the other hand, had no significant effect on profile of tyrosine phosphorylated proteins, which closely resembled that in untreated (resting) platelets (Figure 3c, lanes 1 and 2). We asked next whether G-NH_2 could affect the level of intracellular ROS in human platelets. 2′,7′- Dichlorodihydrofluorescein diacetate (H_2DCF/DA) (20 μM)-loaded platelets were exposed to different concentrations of G-NH_2 at 37 °C for 10 min. There was no significant change in ROS level in platelets exposed to either 2 or 5 μg/mL G-NH_2, while at higher concentration (10 μg/mL), a 2-fold rise in cytosolic ROS was recorded (Figure 3d). The observed elevation in ROS was entirely scavenged by the reductant *N*-acetylcysteine (NAC) (Figure 3d). Contrasting this and expectedly, a lower concentration of GO (2 μg/mL) was sufficient to trigger more than 2-fold enhancement in the level of cytosolic ROS (Figure 3d).[22] H_2O_2 was employed as positive control to increase cytosolic ROS.

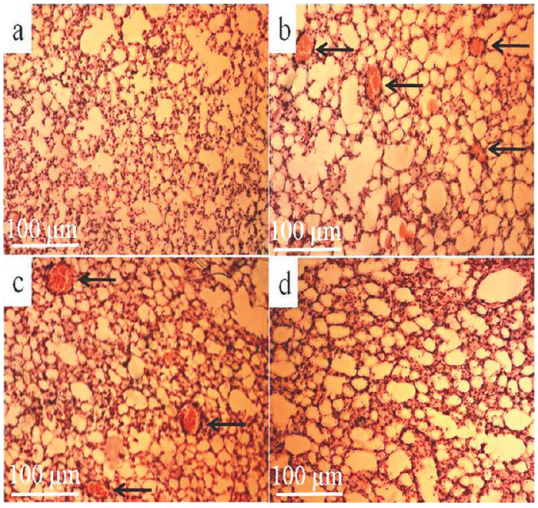

Figure 5. *In vivo* thrombogenecity of graphene. Light microscopy of hematoxylin and eosin stained sections of lungs after intravenous injection of mice with normal saline (a), collagen/epinephrine mixture (b), GO (c), and G-NH_2 (d). Arrows indicate platelet-rich thrombi occluding lung vessels.

Effect of G-NH_2 on Erythrocyte Membrane Integrity. Red blood corpuscles (RBCs) are the most abundant cell population in blood. As nanomaterials finding access into circulation would expose them to circulating RBCs as well as platelets, we sought to determine the effect of G-NH_2 on RBCs. GO has recently been reported to induce significant breakdown of the RBC membrane leading to hemolysis.[28] In line with this, surface membrane of RBCs was progressively compromised by GO in a dose (2–10 μg/mL)-dependent manner, leading to release of free hemoglobin in the medium (Figure 4). Contrasting this, G-NH_2 did not exhibit any hemolytic activity at all even when concentration of G-NH_2 was raised to 50 μg/mL (not shown). We conclude that G-NH_2 is a highly hemocompatible nanomaterial, which does not affect biology of circulating blood cells

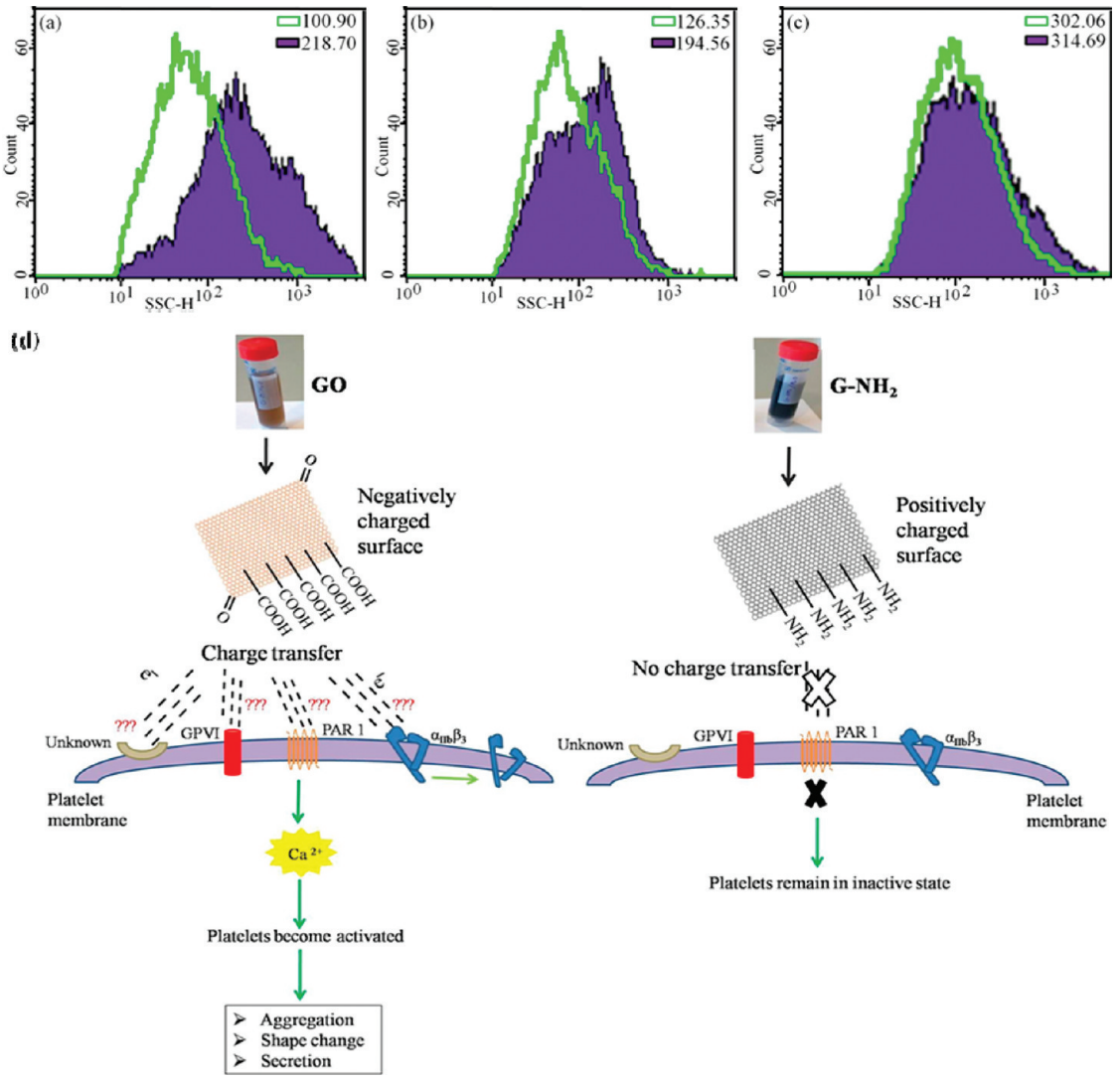

Figure 6. Graphene–platelet interaction. SSC-H histogram plots of GO (a) or RGO (b) or G-NH_2 (c), either untreated (unshaded) or mixed with platelets (shaded). Median values for GO, RGO, and G-NH_2 are stated within corresponding boxes. The number of events analyzed in each case was 10000. The results are representative of five independent experiments. (d) Proposed model for differential effect of GO and G-NH_2 on platelet functions. Surface charge distribution on graphene determines its interaction with platelets. Platelet membranes with different agonist receptors and downstream signaling path are shown.

and maintains both RBCs as well as platelets in a resting state unlike its oxidized counterpart.

Cytotoxicity Assessment of G-NH_2. In order to reaffirm biocompatibility of G-NH_2, its cytotoxicity was assessed from MTT assay. MTT is known to be reduced to formazan in viable cells by mitochondrial reductase exhibiting a purple color. Formazan production was measured after 1 h exposure of platelets to different concentrations (2–20 μg/mL) of G-NH_2 against a control of untreated platelets. G-NH_2 did not induce cell death even when incubated at the highest concentration (20 μg/mL) (Supporting Information Figure S6a). Further, a 24 h exposure of human monocyte cell line, THP-1, to similar concentrations of G-NH_2 failed to significantly alter cell viability. The results supported the conclusion that G-NH_2 did not exhibit long-term cellular toxicity (Supporting Information Figure S6b).

Study of *In Vivo* Thrombogenecity of Parenterally Administered G-NH_2. In order to validate that G-NH_2 had no thrombogenic potential unlike its oxidized counterpart, we studied the effect of either graphene derivatives on thrombus formation in an *in vivo* thrombosis model. GO (250 μg/kg body weight), G-NH_2 (250 μg/kg body weight), a mixture of collagen (200 μg/mL) plus epinephrine (2 μg/mL), or saline was administered intravenously into different groups of mice, and histological sections of lungs were obtained after 15 min. Hematoxylin/eosin stained sections exhibited occlusion of significantly large number of lung vessels (46 $\pm$ 4% and 52 $\pm$ 6%, respectively) with platelet thrombi in mice administered with GO or collagen/epinephrine mixture (positive control), compared to the saline-treated (negative control) mice, which had no occlusion. Contrasting this, pulmonary vessels appeared

normal with absolutely no sign of occlusive pathology in mice administered with G-NH_2 (Figure 5).

Characterization of Graphene–Platelet Interaction. As above observations underscored the lack of interface between G-NH_2 and platelet signaling machinery, which sharply opposed the results obtained with other forms of surface-modified graphene, we explored physical interaction between graphene derivatives and platelets using flow cytometry.[22] Side scattering signals reflect internal complexities of individual as well as interacting particles and are thus a reliable measure of the extent of nanomaterial–cell interaction.[37,38] SSC parameters of GO, RGO, G-NH_2, and corresponding mixtures with platelets were acquired in histogram acquisition plots (Figure 6). Addition of GO (2 μg/mL) to platelets (0.5×10^8/mL) resulted in enhancement in side scatter compared with untreated GO, associated with right shift of the overlaid histogram by 118 $\pm$ 5% (Figure 6a), suggestive of profound physical interaction between GO sheets and platelets. The SSC shift was 53 $\pm$ 2% when a similar number of platelets were incubated with RGO (2 μg/mL) as compared to untreated RGO population (Figure 6b). Remarkably, a mixture of G-NH_2 and platelets at identical concentrations exhibited only a minor shift in SSC (by 3.6 $\pm$ 0.3%), thus underscoring the lack of cellular interaction of G-NH_2 (Figure 6c). Similar results were obtained when side scatter from the graphene–platelet mixture population was compared with that from untreated platelet population (not shown). We infer that GO, which exhibited substantial interaction with cells, elicited activation-specific platelet responses including aggregation, rise in intracellular calcium/ROS, and enhanced protein tyrosine phosphorylation, associated with extensive pulmonary thromboembolism. In contrast, G-NH_2, despite sharing strikingly similar physical attributes (structural morphology, crystallinity, as well as high aqueous dispersibility) with GO, was inert toward cells, did not induce platelet stimulation, and had no demonstrable thrombogenecity *in vivo*.

Surface charge distribution is an important regulator of the physical interface between nanomaterials and a biological system. There have been recent reports suggestive of a correlation between the degree of functionalization or defects on carbon-based nanomaterials and ensuing cytotoxicity.[39–41] Extrinsic defects such as catalyst residue could also be harmful for biomedical applications.[42] We found similar defect characteristics between GO and G-NH_2 despite different surface charge properties (Supporting Information Figures S1 and S2). When correlated with our findings in Figure 3 and Figure 6, these observations indicated that negatively charged graphene sheets physically interacted with platelets and activated them, while positively charged sheets did not. As direct interaction between nanomaterials and cells modulates critical cell signaling pathways and contributes to observed toxicity, modification of surface charge with ensuing diminished effect on nanomaterial–cell interaction can bring about significant attenuation in toxicity. Other approaches to functionalize GO, particularly PEGylation, may not mask all negatively charged –OH or –COOH moieties on GO sheets that are crucial for determining graphene-cell interaction, and hence, PEGylated GO may not be completely free from thrombotoxicity.

CONCLUSION

Although GO has been widely investigated for diverse biomedical applications ranging from cell imaging and drug delivery to photothermal cancer ablation,[3–5,8,9] strong thrombogenecity associated with this material as well as its propensity to induce hemolysis can potentially prohibit its applications. We show here for the first time that, unlike GO, the amine derivative of graphene, G-NH_2, is not endowed with any pro-thrombotic or platelet-stimulating characteristics nor does it compromise integrity of RBCs, which may be attributable to decreased interaction of G-NH_2 with the cells (Figure 6d). Further, in view of its significant absorbance in the NIR region (Supporting Information Figure S1b) and enhanced thermal properties,[43] G-NH_2 can be a potentially strong candidate for photothermal ablation therapy and *in vivo* imaging (photoacoustic imaging).[44–48] Beyond these optical-based applications, G-NH_2 has also been explored in electrochemical biosensing and found to have valuable properties such as wide linear detection range, acceptable reproducibility, high sensitivity, long-term stability, and low detection limit.[49] In conclusion, G-NH_2 is the safest graphene derivative with potential for biomedical applications due to its lack of thrombotic and hemolytic predisposition unlike other graphene derivatives.

METHODS

Synthesis of G-NH_2. GO sheets were prepared by refluxing commercially obtained graphite powder (5 g) with a strongly acidic mixture of sulfuric and nitric acid, as already described.[50,51] The purified GO solution was then freeze-dried and stored in a vacuum oven at room temperature until use.[35,52,53] For preparation of RGO, the freeze-dried GO was charged into a quartz tube and purged with argon for 30 s. Rapid thermal heating (>2000 °C/min) to 1100 °C reduced functional epoxy and hydroxyl groups from the surface of GO sheets through evolution of CO_2. The release of CO_2 inevitably leaves behind vacancies and some residual functional sites that are responsible for the colloidal nature of RGO sheets in the water solutions. For amine functionalization, GO sheets (1 g) were stirred in a mixture of $SOCl_2$ and dimethylformamide (DMF), filtered through a PTFE membrane (pore size 0.2 μm), and washed with dry methylene chloride. The above

procedure led to formation of graphene−COCl, which was dissolved in a mixture of sodium azide (1.5 mM) and DMF at room temperature for 40 h. The reaction product was isolated by filtration and sonicated in concentrated hydrochloric acid to yield graphene−amine product. Finally, the product was washed repeatedly with deionized water until the pH of the filtrate was neutral. Purified G-NH_2 was dispersed in water at the desired concentration (0.05 mg/mL). Similar procedure has been described elsewhere for covalent amine functionalization of carbon nanotubes.[54]

Platelet Preparation. Platelets were isolated by differential centrifugation from fresh human blood, as already described.[55] Briefly, blood from healthy volunteers was collected in citrate-phosphate-dextrose adenine and centrifuged at 180*g* for 20 min. PRP (platelet-rich plasma) was incubated with 1 mM acetylsalicylic acid for 15 min at 37 °C. After addition of ethylenediaminetetraacetic acid (EDTA) (5 mM), platelets were sedimented by centrifugation at 800*g* for 10 min. Cells were washed in buffer A (20 mM HEPES, 138 mM NaCl, 2.9 mM KCl, 1 mM $MgCl_2$, 0.36 mM NaH_2PO_4, 1 mM EGTA (ethylene glycol tetraacetic acid), supplemented with 5 mM glucose, and 0.6 ADPase units of apyrase/mL, pH 6.2). Platelets were finally resuspended in buffer B (pH 7.4), which was the same as buffer A but without EGTA and apyrase. The final cell count was adjusted to $0.5-0.8 \times 10^9$/mL. Morphology of the cells was studied under a fluorescence microscope with a phase contrast attachment (Nikon model Eclipse Ti-E, Towa Optics, India). All steps were carried out under sterile conditions, and precautions were taken to maintain the cells in the inactivated state.

Flow Cytometry. Suspensions of G-NH_2, GO, or RGO as well as platelets were diluted with sheath fluid and analyzed with FACSCalibur flow cytometer (Becton Dickinson India Pvt. Ltd., Gurgaon) fitted with two excitation sources, 488 nm (air-cooled argon-ion laser) and 632 nm (red diode laser), using Cell Quest Pro software. FSC and SSC optical signals, which respectively represent size and granularity of the particles, were acquired in logarithmic scale using primary data acquisition mode. Changes in these particle parameters will modify the quantum of laser light diffracted or scattered, thus causing altered population distribution in FSC−SSC planes. Intensity of fluorescence emission was detected on four separate detectors, labeled FL1, FL2, FL3, and FL4, each with its own set of wavelength filters, and data were presented in the form of histograms. Gate was imposed on all of the graphene derivative population for exclusive analysis. Events were acquired by using collection criteria of the software to stop acquisition after 10000 events were acquired.

Platelet Aggregation Studies. Platelets were stirred (1200 rpm) at 37 °C in a whole blood/optical lumi-aggregometer (Chronolog model 700-2, Wheecon Instruments, India) for 1 min prior to the addition of G-NH_2, GO, or RGO. Aggregation was measured as percent change in light transmission, where 100% refers to transmittance through the blank sample. Finally, cells were boiled in Laemmli lysis buffer and stored at −20 °C until further analysis.

Measurement of Intracellular Free Calcium. PRP was incubated with 2 μM Fura-2 AM for 45 min at 37 °C in the dark. Fura-2-loaded platelets were washed and resuspended in buffer B at 10^8 cells/mL. Fluorescence was recorded in 400 μL aliquots of platelet suspensions at 37 °C under nonstirring conditions using a fluorescence spectrophotometer (Hitachi model F-2500, Techcomp India). Excitation wavelengths were 340 and 380 nm, and emission wavelength was set at 510 nm. Changes in intracellular free calcium concentration, $[Ca^{2+}]_i$, upon addition of GO, RGO, or G-NH_2 at identical concentration (2 μg/mL) were monitored from the fluorescence ratio (340/380) using the Intracellular Cation Measurement Program in FL Solutions software. Intracellular free calcium was calibrated according to the derivation of Grynkiewicz *et al.*[56]

Measurement of Intracellular ROS. H_2DCF-DA, a ROS-sensitive probe, was used to detect oxidative activity in platelets. H_2DCF-DA is known to passively diffuse into cells, where its acetate groups are cleaved by intracellular esterases, releasing the corresponding dichlorodihydrofluorescein (DCF) derivative. Subsequent oxidation by intracellular ROS yields a fluorescent adduct that is trapped inside the cell. Aliquots of platelet suspension (1×10^7 cells/mL) were incubated with 20 μM H_2DCF-DA at 37 °C for 30 min. G-NH_2 (2−10 μg/mL) or GO (2 μg/mL) was added to platelet suspensions 20 min after addition of H_2DCF-DA. Fluorescence was measured with a fluorescence microplate reader (BioTek model FLx800, Medispec India) at 37 °C (excitation, 500 nm; emission, 530 nm). Hydrogen peroxide (10 μM) was added to the platelet suspension as a positive control.

***In Vitro* Hemolysis Assay.** *In vitro* hemolysis assay was carried out as described.[28] Briefly, fresh EDTA-stabilized human whole blood samples were collected from healthy volunteers. Typically, 1 mL of whole blood was added to 2 mL of PBS and centrifuged at 500*g* for 10 min to separate RBCs. The purification step was repeated four times, and washed RBCs were diluted to 10 mL in PBS. To test hemolytic activity of G-NH_2 and GO, 1 mL of RBC suspension ($\sim 0.5 \times 10^8$ cells/mL) was exposed to different concentrations of G-NH_2 and GO in PBS. In order to obtain positive and negative controls, RBCs were suspended either in deionized water or PBS, respectively. Samples were incubated in a rocking shaker at 37 °C for 3 h, followed by centrifugation at 10000*g* for 10 min. Hemoglobin absorbance in the supernatant was measured at 540 nm, with 655 nm as a reference, in a microplate spectrophotometer (BioTek model Power Wave XS2, Medispec India) at 37 °C. Percent hemolysis was calculated using following equation:

$$\text{percent hemolysis } (\%) = \left[\frac{\text{samplesabs}_{540\,-\,655\text{nm}} - \text{negativecontrolabs}_{540\,-\,655\text{nm}}}{\text{positivecontrolabs}_{540\,-\,655\text{nm}} - \text{negativecontrolabs}_{540\,-\,655\text{nm}}}\right] \times 100$$

MTT Assay. MTT assay measures the reduction of a tetrazolium component (MTT) into an insoluble dark-blue formazan product by the mitochondria of viable cells. Cytotoxicity of G-NH_2 against platelets was assessed after 1 h exposure of platelets to different concentrations (2−20 μg/mL) of G-NH_2. After treatment, cells were incubated with 50 μM MTT for an additional 3 h at 37 °C. The soluble formazan formed after reduction of MTT was dissolved in 200 μL of DMSO, and absorbance was measured at 570 nm with a microplate spectrophotometer (BioTek model Power Wave XS2, Medispec India) at 37 °C. For longer duration toxicity study, human monocyte cell line, THP-1, was exposed to similar concentrations of G-NH_2 for 24 h. Culture was processed and subjected to MTT assay as discussed above. Untreated cells were used as a positive control (100% viable) in the study.

Induction of Pulmonary Thromboembolism. Pulmonary thromboembolism was performed in 8−12 week old Swiss male mice, using a method described previously.[57] In control mice, thrombotic challenge was generated by rapid intravenous injection of 150 μL of mixture of collagen−epinephrine into one of the tail veins. In other cases, GO, G-NH_2, or RGO was administered intravenously into mice. After 15 min, the animal was sacrificed by an overdose of anesthesia. Lungs were removed, rinsed in cold saline, and fixed immediately in 10% formalin for at least 24 h. Lung histology was performed and was counted by light microscopy (Nikon model Eclipse Ti-E, Towa Optics, India) in paraffin-embedded sections stained with hematoxylin and eosin.[57] At least 10 fields, at a magnification of 40×, were observed for every specimen.

Statistical Methods. Standard statistical methods were used. Parametric methods (*t* test) were used for evaluation, and significance tests were considered significant at *P* less than 0.05 (2-tailed tests). Data are presented as means ± SD of at least four individual experiments.

Conflict of Interest: The authors declare no competing financial interest.

Acknowledgment. This research was supported by grants received by D. Dash from the Department of Biotechnology (DBT) and the Department of Science and Technology (DST), Government of India, and Indian Council of Medical Research (ICMR). The equipment support from the DST Unit on Nanoscience and Technology (DST-UNANST), Banaras Hindu University (BHU), is gratefully acknowledged. We sincerely thank

Dr. Mohan Kumar, Department of Pathology, IMS, BHU, for helping with the lung histology study. M.K.S. would like to thank the Ciencia 2007 Program, Foundation of Science and Technology (FCT—Portugal) and facility RNME—Pole University of Aveiro. S.K.S. and V.K.S. are recipients of research fellowships from the University Grants Commission and ICMR, New Delhi, respectively. P.P.K. is supported by residency programme of Institute of Medical Sciences, BHU.

Supporting Information Available: Materials used; figures and respective legends for G-NH_2 characterization and MTT assay of G-NH_2-treated platelets. This material is available free of charge *via* the Internet at http://pubs.acs.org.

REFERENCES AND NOTES

1. Wang, Y.; Li, Y. M.; Tang, L. H.; Lu, J.; Li, J. H. Application of Graphene-Modified Electrode for Selective Detection of Dopamine. *Electrochem. Commun.* **2009**, *11*, 889–892.
2. Liu, Y.; Yu, D.; Zeng, C.; Miao, Z.; Dai, L. Biocompatible Graphene Oxide-Based Glucose Biosensors. *Langmuir* **2010**, *26*, 6158–6160.
3. Peng, C.; Hu, W.; Zhou, Y.; Fan, C.; Huang, Q. Intracellular Imaging with a Graphene-Based Fluorescent Probe. *Small* **2010**, *6*, 1686–1692.
4. Sun, X.; Liu, Z.; Welsher, K.; Robinson, J. T.; Goodwin, A.; Zaric, S.; Dai, H. Nano-Graphene Oxide for Cellular Imaging and Drug Delivery. *Nano Res.* **2008**, *1*, 203–212.
5. Liu, Z.; Robinson, J. T.; Sun, X.; Dai, H. PEGylated Nano-Graphene Oxide for Delivery of Water Insoluble Cancer Drugs. *J. Am. Chem. Soc.* **2008**, *130*, 10876–10877.
6. Hu, W.; Peng, C.; Luo, W.; Lv, M.; Li, X.; Li, D.; Huang, Q.; Fan., C. Graphene-Based Antibacterial Paper. *ACS Nano* **2010**, *4*, 4317–4323.
7. Akhavan, O.; Ghaderi, E. Toxicity of Graphene and Graphene Oxide Nanowalls against Bacteria. *ACS Nano* **2010**, *4*, 5731–5736.
8. Yang, K.; Zhang, S.; Zhang, G.; Sun, X.; Lee, S. T.; Liu, Z. Graphene in Mice: Ultrahigh *In Vivo* Tumor Uptake and Efficient Photothermal Therapy. *Nano Lett.* **2010**, *10*, 3318–3323.
9. Robinson, J. T.; Tabakman, S. M.; Liang, Y.; Wang, H.; Casalongue, S. H.; Vinh, D.; Dai, H. Ultrasmall Reduced Graphene Oxide with High Near-Infrared Absorbance for Photothermal Therapy. *J. Am. Chem. Soc.* **2011**, *133*, 6825–6831.
10. Shan, C.; Yang, H.; Han, D.; Zhang, Q.; Ivaska, A.; Niu, L. Water-Soluble Graphene Covalently Functionalized by Biocompatible Poly-L-Lysine. *Langmuir* **2009**, *25*, 12030–12033.
11. Luo, J.; Cote, L. J.; Tung, V. C.; Tan, A. T. L.; Goins, P. E.; Wu, J.; Huang, J. Graphene Oxide Nanocolloids. *J. Am. Chem. Soc.* **2010**, *132*, 17667–17669.
12. Zhang, L.; Xia, J.; Zhao, Q.; Liu, L.; Zhang, Z. Functional Graphene Oxide as a Nanocarrier for Controlled Loading and Targeted Delivery of Mixed Anticancer Drugs. *Small* **2009**, *6*, 537–544.
13. Yang, X.; Zhang, X.; Liu, Z.; Ma, Y.; Huang, Y.; Chen, Y. High-Efficiency Loading and Controlled Release of Doxorubicin Hydrochloride on Graphene Oxide. *J. Phys. Chem. C* **2008**, *112*, 17554–17558.
14. He, S.; Song, B.; Li, D.; Zhu, C.; Qi, W.; Wen, Y.; Wang, L.; Song, S.; Fang, H.; Fan, C. A Graphene Nanoprobe for Rapid, Sensitive, and Multicolor Fluorescent DNA Analysis. *Adv. Funct. Mater.* **2010**, *20*, 453–459.
15. Jung, J. H.; Cheon, D. S.; Liu, F.; Lee, K. B.; Seo, T. S. A Graphene Oxide Based Immuno-Biosensor for Pathogen Detection. *Angew. Chem., Int. Ed.* **2010**, *49*, 5708–5711.
16. He, Q. Y.; Sudibya, H. G.; Yin, Z. Y.; Wu, S. X.; Li, H.; Boey, F.; Huang, W.; Chen, P.; Zhang, H. Centimeter-Long and Large-Scale Micropatterns of Reduced Graphene Oxide Films: Fabrication and Sensing Applications. *ACS Nano* **2010**, *4*, 3201–3208.
17. Wang, Z. J.; Zhou, X. Z.; Zhang, J.; Boey, F.; Zhang, H. Direct Electrochemical Reduction of Single-Layer Graphene Oxide and Subsequent Functionalization with Glucose Oxidase. *J. Phys. Chem. C* **2009**, *113*, 14071–14075.
18. Saller, F.; Schapira, M.; Angelillo-Scherrer, A. Role of Platelet Signaling in Thrombus Stabilization: Potential Therapeutic Implications. *Curr. Signal Transduction Ther.* **2008**, *3*, 22–54.
19. Badruddin, A.; Gorelick, P. B. Antiplatelet Therapy for Prevention of Recurrent Stroke. *Curr. Treat. Options Neurol.* **2009**, *11*, 452–459.
20. Weston, C.; Rao, U. Antiplatelet Drugs in Cardiovascular Diseases. *Int. J. Clin. Pract.* **2003**, *57*, 898–905.
21. Talavera, Y. A.; Hernandez, I. M.; Portilla, C. V. Platelet Activation: Basic Aspects, Its Role in Cerebrovascular Disease and Its Therapeutic Projections. *Revista Ecuatoriana de Neurologia* **2007**, *16*, 127–132.
22. Singh, S. K.; Singh, M. K.; Nayak, M. K.; Kumari, S.; Shrivastava, S.; Gracio, J. A.; Dash, D. Thrombus Inducing Property of Atomically Thin Graphene Oxide Sheets. *ACS Nano* **2011**, *5*, 4987–4996.
23. Wang, K.; Ruan, J.; Song, H.; Zhang, J.; Wo, Y.; Guo, S.; Cui, D. Biocompatibility of Graphene Oxide. *Nanoscale Res. Lett.* **2011**, *6*, 8–15.
24. Agarwal, S.; Zhou, X.; Ye, F.; He, Q.; Chen, G. C. K.; Soo, J.; Beoy, F.; Zhang, H.; Chen, P. Interfacing Live Cells with Nanocarbon Substrates. *Langmuir* **2010**, *26*, 2244–2247.
25. Chang, Y.; Yanga, S.-T.; Liua, J.-H.; Dong, E.; Wang, Y.; Cao, A.; Liu, Y.; Wang, H. *In Vitro* Toxicity Evaluation of Graphene Oxide on A549 Cells. *Toxicol. Lett.* **2011**, *200*, 201–210.
26. Yang, K.; Wan, J.; Zhang, S.; Zhang, Y.; Lee, S.-T.; Liu, Z. *In Vivo* Pharmacokinetics, Long-Term Biodistribution, and Toxicology of PEGylated Graphene in Mice. *ACS Nano* **2011**, *5*, 516–522.
27. Zhang, X.; Yin, J.; Peng, C.; Hu, W.; Zhu, Z.; Li, W.; Fan, C.; Huan, Q. Distribution and Biocompatibility Studies of Graphene Oxide in Mice after Intravenous Administration. *Carbon* **2011**, *49*, 986–995.
28. Liao, K.-H.; Lin, Y.-S.; Macosko, C. W.; Haynes, C. L. Cytotoxicity of Graphene Oxide and Graphene in Human Erythrocytes and Skin Fibroblasts. *ACS Appl. Mater. Interfaces* **2011**, *3*, 2607–2615.
29. Lee, H. J.; Park, J.; Yoon, O. J.; Kim, H. W.; Lee, D. Y.; Kim, D. H.; Lee, W. B.; Lee, N.-E.; Bonventre, J. V.; Kim, S. S. Amine-Modified Single-Walled Carbon Nanotubes Protect Neurons from Injury in a Rat Stroke Model. *Nat. Nanotechnol.* **2011**, *6*, 121–125.
30. Lee, W.; Parpura, V. Wiring Neurons with Carbon Nanotubes. *Front. Neuroeng.* **2009**, *2*, 1–3.
31. Reddy, A. L. M.; Srivastava, A.; Gowda, S. R.; Gullapalli, H.; Dubey, M.; Ajayan, P. M. Synthesis of Nitrogen-Doped Graphene Films for Lithium Battery Application. *ACS Nano* **2010**, *4*, 6337–6342.
32. Misra, A.; Tyagi, P. K.; Singh, M. K.; Misra, D. S. FTIR Studies of Nitrogen Doped Carbon Nanotubes. *Diamond Relat. Mater.* **2006**, *15*, 385–388.
33. Fang, M.; Zhang, Z.; Li, J.; Zhang, H.; Lu, H.; Yang, J. Y. Constructing Hierarchically Structured Interphases for Strong and Tough Epoxy Nanocomposites by Amine-Rich Graphene Surfaces. *Mater. Chem.* **2010**, *20*, 9635–9643.
34. Park, J. S.; Cho, S. M.; Kim, W.-J.; Park, J.; Yoo, P. J. Fabrication of Graphene Thin Films Based on Layer-By-Layer Self-Assembly of Functionalized Graphene Nanosheets. *ACS Appl. Mater. Interfaces* **2011**, *3*, 360–368.
35. Singh, S. K.; Singh, M. K.; Nayak, M. K.; Kumari, S.; Gracio, J. A.; Dash, D. Size Distribution Analysis and Physical/Fluorescence Characterization of Graphene Oxide Sheets by Flow Cytometry. *Carbon* **2011**, *49*, 684–692.
36. Sun, X.; Luo, D.; Liu, J.; Evans, D. G. Monodisperse Chemically Modified Graphene Obtained by Density Gradient Ultracentrifugal Rate Separation. *ACS Nano* **2010**, *4*, 3381–3389.
37. Sasidharan, A.; Panchakarla, L. S.; Chandran, P.; Menon, D.; Nair, S.; Rao, C. N. R.; Koyakutty, M. Differential Nano-Bio Interactions and Toxicity Effects of Pristine *versus* Functionalized Graphene. *Nanoscale* **2011**, *3*, 2461–2464.
38. Cai, D.; Blair, D.; Dufort, F. J.; Gumina, M. R.; Huang, Z.; Hong, G.; Wagner, D.; Canahan, D.; Kempa, K.; Ren, Z. F.; *et al.* Interaction between Carbon Nanotubes and Mammalian

Cells: Characterization by Flow Cytometry and Application. *Nanotechnology* **2008**, *19*, 345102–345111.
39. Magrez, A.; Kasas, S.; Salicio, V.; Pasquier, N.; Seo, J. W.; Celio, M.; Catsicas, S.; Schwaller, B.; Forro, L. Cellular Toxicity of Carbon-Based Nanomaterials. *Nano Lett.* **2006**, *6*, 1121–1125.
40. Yu, X.; Cai, H.; Zhang, W.; Li, X.; Pan, N.; Luo, Y.; Wang, X.; Hou, J. G. Tuning Chemical Enhancement of SERS by Controlling the Chemical Reduction of Graphene Oxide Nanosheets. *ACS Nano* **2011**, *5*, 952–958.
41. Sanchez, V. C.; Jachak, A.; Hurt, R. H.; Kane, A. B. Biological Interactions of Graphene-Family Nanomaterials: An Interdisciplinary Review. *Chem. Res. Toxicol.* **2012**, *25*, 15–34.
42. Pulskamp, K.; Diabaté, S.; Krug, H. F. Carbon Nanotubes Show No Sign of Acute Toxicity but Induce Intracellular Reactive Oxygen Species in Dependence on Contaminants. *Toxicol. Lett.* **2007**, *168*, 58–74.
43. Hu, Y.; Shen, J.; Li, N.; Shi, M.; Ma, H.; Yan, B.; Wang, W.; Huang, W.; Ye, M. Amino-Functionalization of Graphene Sheets and the Fabrication of Their Nanocomposites. *Polym. Compos.* **2010**, *31*, 1987–1994.
44. Xu, M. H.; Wang, L. H. V. Photoacoustic Imaging in Biomedicine. *Rev. Sci. Instrum.* **2006**, *77*, 041101–041122.
45. Zerda, A.; Zavaleta, C.; Keren, S.; Vaithilingam, S.; Bodapati, S.; Liu, Z.; Levi, J.; Ma, T. J.; Oralkan, O.; Cheng, Z.; *et al.* Photoacoustic Molecular Imaging in Living Mice Utilizing Targeted Carbon Nanotubes. *Nat. Nanotechnol.* **2008**, *3*, 557–562.
46. Tian, B.; Wang, C.; Zhang, S.; Feng, L.; Liu, Z. Photothermally Enhanced Photodynamic Therapy Delivered by Nano-Graphene Oxide. *ACS Nano* **2011**, *5*, 7000–7009.
47. Zhang, W.; Guo, Z.; Huang, D.; Liu, Z.; Guo, X.; Zhong, H. Synergistic Effect of Chemo-Photothermal Therapy Using PEGylated Graphene Oxide. *Biomaterials* **2011**, *32*, 8555–8561.
48. Yang, K.; Wan, J.; Zhang, S.; Tian, B.; Zhang, Y.; Liu, Z. The Influence of Surface Chemistry and Size of Nanoscale Graphene Oxide on Photothermal Therapy of Cancer Using Ultra-Low Laser Power. *Biomaterials* **2012**, *33*, 2206–2214.
49. Huang, K.-J.; Niu, D.-J.; Liu, X.; Wu, Z.-W.; Yang, F.; Chang, Y.-F.; Wu, Y.-Y. Direct Electrochemistry of Catalase at Amine-Functionalized Graphene/Gold Nanoparticles Composite Film for Hydrogen Peroxide Sensor. *Electrochim. Acta* **2011**, *56*, 2947–2953.
50. Singh, M. K.; Titus, E.; Gonçalve, G.; Marques, P. A. A. P.; Bdikin, I.; Kholkin, A. L.; Gracio, J. J. A. Atomic-Scale Observation of Rotational Misorientation in Suspended Few Layer Graphene Sheets. *Nanoscale* **2010**, *2*, 700–708.
51. Gonçalves, G.; Marques, P. A. A. P.; Barros-Timmons, A.; Bdikin, I.; Singh, M. K.; Emamic, N.; Gracio, J. Graphene Oxide Modified with PMMA *via* ATRP as Reinforcement Filler. *J. Mater. Chem.* **2010**, *20*, 9927–9934.
52. Singh, M. K.; Shokuhfar, T.; Gracio, J.; Sousa, A. C. M.; Fereira, J. M.; Garmestani, H.; Ahzi, S. Carbon Nanotube-Reinforced PMMA Modified HA: A Novel Nanocomposite Material for Biomedical Applications. *Adv. Funct. Mater.* **2008**, *18*, 694–700.
53. Singh, M. K.; Gracio, J.; LeDuc, P.; Gonçalves, P.; Marques, P.; Gonçalves, G.; Marques, F.; Silva, V.; Silva, F. C. E.; Potes, J.; *et al.* Integrated Biomimetic Carbon Nanotube Composites for *In Vivo* Systems. *Nanoscale* **2010**, *2*, 2855–2863.
54. Ramanathan, T.; Fisher, F. T.; Ruoff, R. S.; Brinson, L. C. Amino-Functionalized Carbon Nanotubes for Binding to Polymers and Biological Systems. *Chem. Mater.* **2005**, *17*, 1290–1295.
55. Shrivastava, S.; Bera, T.; Singh, S. K.; Singh, G.; Ramachandrarao, P.; Dash, D. Characterization of Novel Anti-Platelet Properties of Silver Nanoparticles. *ACS Nano* **2009**, *3*, 1357–1364.
56. Grynkiewicz, G.; Poenie, M.; Tsien, R. Y. A New Generation of Ca^{2+} Indicators with Greatly Improved Fluorescence Properties. *J. Biol. Chem.* **1985**, *260*, 3440–3450.
57. Momi, S.; Falcinelli, E.; Giannini, S.; Ruggeri, L.; Cecchetti, L.; Corazzi, T.; Libert, C.; Gresele, P. Loss of Matrix Metalloproteinase 2 in Platelets Reduces Arterial Thrombosis *in Vivo*. *J. Exp. Med.* **2009**, *206*, 2365–2379.